Ambidentate coordination in hydrogen bonded dimethyl sulfoxide, $(CH_3)_2SO \cdots H_3O^+$, and in dichlorobis(dimethyl sulfoxide) palladium(II) and platinum(II) solid solvates, by vibrational and sulfur K-edge X-ray absorption spectroscopy†

Emiliana Damian Risberg,[a] János Mink,[b,c] Alireza Abbasi,[a,d] Mikhail Yu. Skripkin,[a,f] Laszló Hajba,[b,c] Patric Lindqvist-Reis,[e] Éva Bencze[b,c] and Magnus Sandström*[a]

Received 18th August 2008, Accepted 23rd October 2008
First published as an Advance Article on the web 13th January 2009
DOI: 10.1039/b814252a

The strongly hydrogen bonded species $(CH_3)_2SO \cdots H_3O^+$ formed in concentrated hydrochloric acid displays a new low energy feature in its sulfur K-edge X-ray absorption near edge structure (XANES) spectrum. Density Functional Theory-Transition Potential (DFT-TP) calculations reveal that the strong hydrogen bonding decreases the energy of the transition S(1s) → LUMO, which has antibonding σ*(S–O) character, with about 0.8 eV. Normal coordinate force field analyses of the vibrational spectra show that the SO stretching force constant decreases from 4.72 N cm^{-1} in neat liquid dimethyl sulfoxide to 3.73 N cm^{-1} for the hydrogen bonded $(CH_3)_2SO \cdots H_3O^+$ species. The effects of sulfur coordination on the ambidentate dimethyl sulfoxide molecule were investigated for the *trans*-Pd$((CH_3)_2SO)_2Cl_2$, *trans*-Pd$((CD_3)_2SO)_2Cl_2$ and *cis*-Pt$((CH_3)_2SO)_2Cl_2$ complexes with square planar coordination of the chlorine and sulfur atoms. The XANES spectra again showed shifts toward low energy for the transition S(1 s) → LUMO, now with antibonding σ*(M–Cl, M–S) character, with a larger shift for M = Pt than Pd. DFT-TP calculations indicated that the differences between the XANES spectra of the geometrical *cis* and *trans* isomers of the M$((CH_3)_2SO)_2Cl_2$ complexes are expected to be too small to allow experimental distinction. The vibrational spectra of the palladium(II) and platinum(II) complexes were recorded and complete assignments of the fundamentals were achieved. Even though the M–S bond distances are quite similar the high covalency especially of the Pt–S bonds induces significant increases in the S–O stretching force constants, 6.79 and 7.18 N cm^{-1}, respectively.

Introduction

Platinum metals are widely used as catalysts in numerous chemical and technological processes such as selective oxidation of exhaust gases from car engines, stereo-selective hydrogenation of non-saturated organic compounds, *etc*. The square planar coordination geometry of palladium(II) and platinum(II) complexes allows easy formation of reaction intermediates *via* non-occupied axial positions. Platinum and palladium are relatively rare noble metals and their separation and recovery from used catalysts are important issues, where solvents with different affinity to the metal ions can be important.

Dimethyl sulfoxide, $(CH_3)_2SO$, is of special interest because of its unusual properties. The ambidentate solvent molecule is able to coordinate to metal ions *via* either the oxygen or the sulfur atom. Oxygen coordination is the more common and the structural and spectroscopic features of such metal complexes have been widely studied.[1–4] Less is known about the sulfur-coordinated complexes that are formed with some soft metal ions. Crystallographic studies indicate that in complexes with platinum(II) ions at most two M–S bonds to dimethyl sulfoxide ligands are formed for steric reasons depending on the other ligands, and additional $(CH_3)_2SO$ molecules will coordinate *via* oxygen.[1,5–8] In vibrational IR absorption spectra the characteristic upshift to 1100–1160 cm^{-1} of the band assigned to S–O stretching, at 1070 cm^{-1} for neat dimethyl sulfoxide, signifies sulfur coordination. However, in covalent complexes vibrational skeletal modes are often extensively coupled, which makes comparisons of the bond character based only on frequency shifts ambiguous. In the low frequency region, the assignment of vibrational fundamentals often becomes tentative without isotopic substitution studies.

[a]*Department of Physical, Inorganic and Structural Chemistry, Stockholm University, SE-106 91, Stockholm, Sweden. E-mail: magnuss@struc.su.se*
[b]*Department of Molecular Spectroscopy, Chemical Research Center of the Hungarian Academy of Sciences, P. O. Box 77, H-1525 Budapest, Hungary*
[c]*Faculty of Information Technology, Research Institute of Chemical and Process Engineering, University of Pannonia, P. O. Box 158, H-8201 Veszprém, Hungary*
[d]*School of Chemistry, University College of Science, University of Tehran, Tehran, Iran*
[e]*Institut für Nukleare Entsorgung, Forschungszentrum Karlsruhe, P.O. Box 3640, D-76021, Karlsruhe, Germany*
[f]*Department of General and Inorganic Chemistry, Saint-Petersburg State University, Universitetsky pr. 26, 198504, Saint-Petersburg, Russia*

† Electronic supplementary information (ESI) available: Table S1 lists the refined force constants for *trans*-$PdCl_2(Me_2SO)_2$ and *cis*-$PtCl_2(Me_2SO)_2$ complexes. Fig. S1 shows the shapes of the receiving MOs for the protonated dimethyl sulfoxide molecule corresponding to transitions **1**, **2**, **3** and **4** in Fig. 6. Figs S2 and S3 display the MOs corresponding to the marked transitions in the theoretical spectra of the *cis*- and *trans*-isomers of the M$(CH_3)_2SO)_2Cl_2$ complexes for M = Pt and Pd in Fig. 7 and 8, respectively. See DOI: 10.1039/b814252a

For the sulfur-coordinated *trans*-$PdX_2((CH_3)_2SO)_2$ (X = Cl, Br) complexes the only comprehensive study so far is that of Tranquille and Forel.[9,10] However, not all vibrational bands were resolved and some revision seems desirable. In the present work normal coordinate force field analyses of the solid state vibrational spectra were performed for the *trans*-$PdCl_2((CH_3)_2SO)_2$ and *cis*-$PtCl_2((CH_3)_2SO)_2$ complexes to enable comparisons of the character of the metal–sulfur and metal–chloride bonding in square planar coordination. The results are combined with sulfur K-edge XANES measurements, which when evaluated by DFT-TP calculations provide information about the electronic state of the investigated compounds. This method was previously applied to study oxygen-coordinated dimethyl sulfoxide solvates,[11] and is in the current work complemented with a study of the hydrogen bonded dimethyl sulfoxide molecule in concentrated hydrochloric acid, combining experimental XANES and vibrational spectra with theoretical computations. The electronic transitions were investigated for several possible models for protonated $(CH_3)_2SO$ species ($(CH_3)_2SOH^+$: $H_2O\cdots{}^+HOS(CH_3)_2$ and $H_2OH^+\cdots OS(CH_3)_2$), and also for the other geometrical isomer of the *cis*-$Pd((CH_3)_2SO)_2Cl_2$ and *trans*-$Pt((CH_3)_2SO)_2Cl_2$ solvates.

Experimental

Sample preparation

Two solutions, of *ca.* 0.05 mol dm^{-3} dimethyl sulfoxide dissolved in acetonitrile and concentrated hydrochloric acid, respectively, were prepared. Complexes of *cis*-$Pt((CH_3)_2SO)_2Cl_2$ (yellow crystals) and *trans*-$Pd((CH_3)_2SO)_2Cl_2$ (orange powder) were synthesized by dissolving anhydrous platinum(II) and palladium(II) chloride, respectively, in dimethyl sulfoxide (heated to about 100 °C for $PdCl_2$) followed by slow cooling to room temperature.[12,13] The compounds were identified by single crystal X-ray diffraction measurements of their cell parameters.[12,13]

Vibrational spectra

Raman spectra of the solid compounds were obtained using a Renishaw System 1000 spectrometer, equipped with a Leica DMLM microscope, a 25 mW diode laser (780 nm), and a Peltier-cooled CCD detector. Mid-infrared (200–4000 cm^{-1}, resolution 4 cm^{-1}, 128 scans) absorption spectra were recorded in a purged atmosphere from nujol mulls on CsI windows using a Bio-Rad (Varian) FTS 175 dynamically aligned spectrometer equipped with a CsI beamsplitter. Far-infrared spectra (50–700 cm^{-1}) were obtained with polyethylene pellets in a Bio-Rad (Varian) FTS-40 air bearing interferometer equipped with a wire-mesh beamsplitter, high pressure mercury source and DTGS detector. All spectra were measured at ambient temperature. To study the effects of hydration and hydrogen bonding on the dimethyl sulfoxide molecule, IR and Raman spectra were recorded of 0.5 mol dm^{-3} dimethyl sulfoxide solutions in water and in concentrated hydrochloric acid (37%). For Raman measurements a dedicated Bio-Rad (Varian) FT Raman spectrometer was used, equipped with a Spectra Physics Nd:YAG laser source (1064 nm wavelength) and a liquid nitrogen-cooled Ge detector. Careful subtraction of corresponding aqueous HCl solution spectra was performed to remove the background from that obtained in the experiment with dimethyl sulfoxide. The experimental spectra are presented in Fig. 1–4 and the vibrational frequencies are listed together with the potential energy distribution (PED) in Table 1–3.

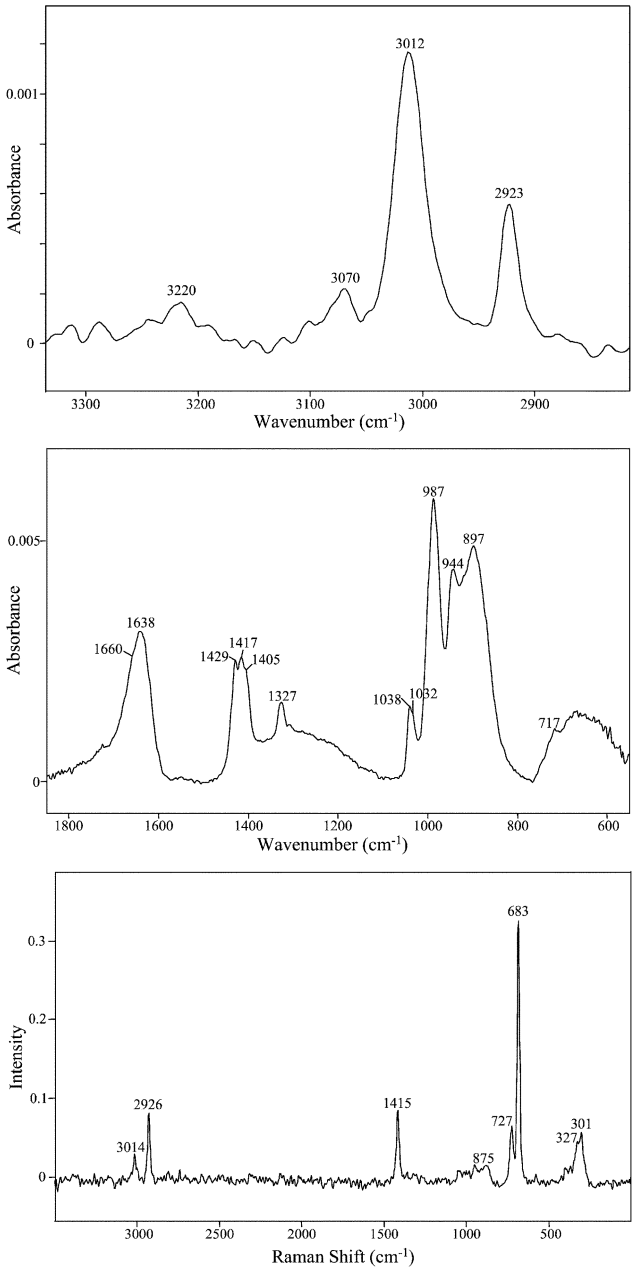

Fig. 1 (Upper, middle) FT-IR difference spectrum of $(CH_3)_2SO$ in HCl solution, after subtraction of the spectrum of HCl(aq); (lower) Raman difference spectrum of $(CH_3)_2SO$ in HCl solution, after subtraction of HCl(aq).

Force field analysis

The $M((CH_3)_2SO)_2Cl_2$ (M = Pd, Pt) complexes contain 23 atoms generating 63 fundamental vibrational modes when including the methyl hydrogens. Detailed analysis of methyl C–H stretching, deformation, rocking and torsional modes are less important in coordination studies than the ligand 'skeletal' modes and the

Table 1 Vibrational transitions (cm^{-1}) in the spectra of dimethyl sulfoxide in liquid and gas phase compared with Me_2SO(aq) and Me_2SO(HCl) after subtraction of the solvent contribution[a]

Me_2SO (gas)[3,9]	Me_2SO (liquid)[3]		Me_2SO(aq)[b]		((Me_2SO in HCl) – HCl(aq)[b]		
IR	IR	Raman	IR	Raman	IR	Raman	Assignment
3010	2991 w	2996 m	2999 w	3000 w	3013 w	3014 w	$\nu_a(CH_3)$
	2983 w		2969 sh			2970 vw	$\nu_a(CH_3)$
2933	2905 w	2913 m	2915 w	2915 w	2923 w	2925 m	$\nu_s(CH_3)$
						2810 vvw	
						2740 vvw	
					1725 vvw		
			1662 w		1660 vvw		$\delta(H_2O)$
			1638 sh		1638 vw, sh		$\delta(H_2O)$
	1437 w		1438 sh		1429 w		$\delta_a(CH_3)$
1419	1419 w	1418 w	1420 sh	1419 m	1417 vw	1415 vw	$\delta_a(CH_3)$
1406	1406 w		1406 w		1405 w		$\delta_a(CH_3)$
1319					1327 w		$\delta_s(CH_3)$
1304	1311 w	1308 w	1312 w	1311 w			$\delta_s(CH_3)$
	1294 sh						$\delta_s(CH_3)$
1102	1070 s	1067 w	1024 vs	1028 sh	987 m		ν(SO), r(CH_3)
1056			1060 sh	1058 sh			r(CH_3)
			1046 sh	1045 m	1038 w		r(CH_3)
1021	1032 m	1029 w			1032 vw, sh		r(CH_3)
1016	1012 m	1010 w					r(CH_3)
953	957 w	957 w	954 sh	953 w	944 sh		ν(SO), r(CH_3)
			932 m	930 sh	919 sh		ν(SO), r(CH_3)
			898 w		897 w		ν(SO), r(CH_3)
						875 vw	
695	700 w	698 m	701 m	701 m	717 vw	727 m	$\nu_a(SC_2)$
					686 vvw	683 s	$\nu_s(SC_2)$
672	670 w	668 s	669 m	671 s	668 vvw		$\nu_s(SC_2)$
382	383 w	382 m		384 w			$\delta(SC_2)$
333	335 w	322 m		335 m		327 w	$\tau(SC_2)$
308	307 w	306 m		307 w		301 w	$\omega(SC_2)$

[a] Notations: ν = stretching, δ = bending, τ = twisting, ω = wagging, r = rocking, s = symmetric, a = asymmetric modes unassigned band belong to overtones and combination modes; intensities: s = strong, m = medium, w = weak, sh = shoulder. [b] This work.

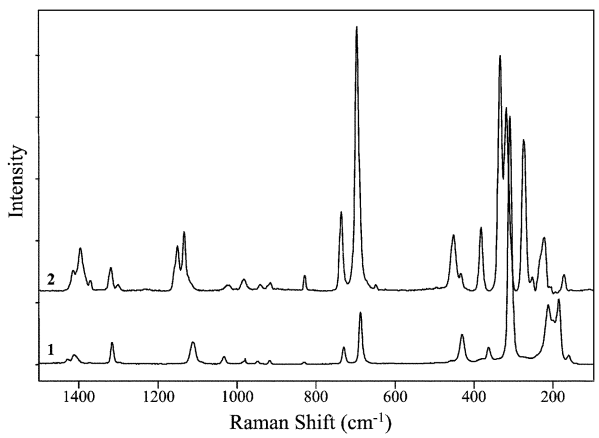

Fig. 2 Raman spectra of the solid *trans*-Pd($(CH_3)_2SO)_2Cl_2$ (**1**) and *cis*-Pt($(CH_3)_2SO)_2Cl_2$ (**2**) compounds.

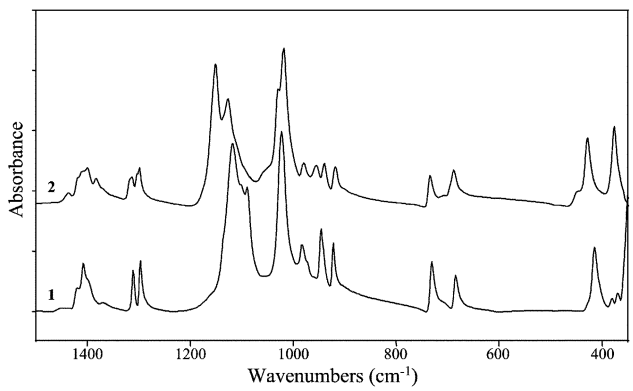

Fig. 3 Mid-IR spectra of the solid *trans*-Pd($(CH_3)_2SO)_2Cl_2$ (**1**) and *cis*-Pt($(CH_3)_2SO)_2Cl_2$ (**2**) compounds.

metal–ligand vibrations. Therefore, point masses (16 and 19 a.m.u. for CH_3 and CD_3, respectively) were introduced for the methyl groups to simplify the calculations, which leaves 27 fundamental modes for the $M(Me_2SO)_2Cl_2$ complexes.

The molecular structure of the complexes was adopted from the literature,[12,13] and the *trans*-Pd($Me_2SO)_2Cl_2$ complex was treated in the C_i point group that results in 12 A_g and 15 A_u vibrations. All A_g vibrations are Raman active whereas the IR active A_u modes should not coincide in the vibrational spectra; a significant help in the assignment. The *cis*-Pt($Me_2SO)_2Cl_2$ complex has in the C_s point group 14 A′ and 13 A″ vibrational modes, all active both in the Raman and IR spectra. However, their intensity difference facilitates the assignment.

For the force field calculations the same set of symmetry coordinates as previously was used for the dimethyl sulfoxide molecule with an initial set of force constants derived from our previous work,[2,3] and for the H_3O^+ ion C_{3v} point group symmetry was adopted. Wilson's **GF** matrix method was used to calculate vibrational frequencies using a symmetrized valence force field.

Table 2 Experimental and calculated (in point groups C_i and C_s), fundamental vibrational frequencies (cm^{-1}) for *trans*-$Pd(Me_2SO)_2Cl_2$ and *cis*-$Pt(Me_2SO)_2Cl_2$, respectively, and their potential energy distribution (PED in %) in symmetry coordinates[a]

trans-$Pd(Me_2SO\text{-}h_6)_2Cl_2$			*trans*-$Pd(Me_2SO\text{-}d_6)_2Cl_2$			*cis*-$Pt(Me_2SO)_2Cl_2$					
IR (A_u)	Raman (A_g)	Calc.	IR (A_u)	Raman (A_g)	Calc.	IR	Raman		Calc.	PED[b]	Assignment
	1110 m	1110		1117 m	1115	1128 s	1132 m	A′	1130	96 ν_s(SO)	ν_s(SO)
1117 s		1117	1119 s		1119	1151 s	1151 m	A″	1150	96 ν_a(SO)	ν_a(SO)
731 m		731		645 m	643	735 s		A″	735	92 ν_a(CS), 5 $\tau_a(SC_2)$	$\nu_a(SC_2)$ – oop
	729 m	729	644 m		646		737 m	A′	737	92 ν_a(CS), 5 $\tau_s(SC_2)$	$\nu_a(SC_2)$ – ip
	688 s	688		631 s	630	697 w	696 s	A′	696	89 ν_s(CS), 5 $\delta_s(SC_2)$	$\nu_s(SC_2)$ – ip
685 m		685	631 m		630	689		A″	689	*Pd*: 91 ν_s(CS) *Pt*: 88 ν_s(CS), 5 ν_s(PtS), 5 $\delta_s(SC_2)$	$\nu_s(SC_2)$ – oop
	431 m	430		389 m	386	449 sh	452 m	A′	452	*Pd*: 71 $\delta_s(SC_2)$, 17 ν_s(PdS), 8 ν_s(CS) *Pt*: 72 $\delta_s(SC_2)$, 21 ν_s(PtS)	$\delta_s(SC_2)$
416 s		416	377 s		375	430 s	433 w	A″	431	*Pd*: 53 $\delta_a(SC_2)$, 41 ν_a(PdS), 5 ν_s(CS) *Pt*: 58 $\delta_a(SC_2)$, 34 ν_a(PtS), 5 ν_s(CS)	$\delta_a(SC_2)$
	381 w	383		365 w	363		381 m	A′	381	84 $\tau_s(SC_2)$, 7 ν_a(CS)	$\tau_s(SC_2)$
382 m		382	367 m		364	376 s	378 w	A″	376	85 $\tau_a(SC_2)$, 6 ν_a(CS)	$\tau_a(SC_2)$
	363 w	363		302 sh	304		319 s	A′	319	95 $\omega_s(SC_2)$	$\omega_s(SC_2)$
330 m		331	288 m		285	320 s		A″	319	94 $\omega_a(SC_2)$	$\omega_a(SC_2)$
354 s		356	337 s		335	309 s	309 m	A″	308	*Pd*: 92 ν_a(PdCl), 6 $r_{\perp a}(SC_2)$ *Pt*: 82 ν_a(PtCl), 11 $\delta_a(SC_2)$	ν_a(MCl)
	309 vs	309		307 vs	306	335 s	335 vs	A′	334	*Pd*: 100 ν_s(PdCl) *Pt*: 91 ν_s(PtCl), 5 $\delta_s(SC_2)$	ν_s(MCl)
246 m		246	245 m		243	251 w	251 m	A″	249	*Pd*: 47 ν_a(PdS), 29 $\delta_a(SC_2)$, 14 $r_{\parallel a}(SC_2)$, 5 $\varphi(PdS_2)$ *Pt*: 59 ν_a(PtS), 23 $\delta_a(SC_2)$, 10 ν_a(PtCl), 6 $r_{\parallel a}(SC_2)$	ν_a(MS)
	160 m	157		152 m	148	273 w	275 s	A′	270	*Pd*: 63 ν_s(PdS), 28 $\delta_s(SC_2)$, 9 $r_{\parallel s}(SC_2)$ *Pt*: 70 ν_s(PtS), 14 $r_{\parallel s}(SC_2)$, 5 φ_s(SPtCl)	ν_s(MS)
	213 m	214		201 m	197	218 sh	221 m	A′	213	*Pd*: 82 $r_{\parallel s}(SC_2)$, 9 ν_s(PdS), 8 $\delta_s(SC_2)$ *Pt*: 46 $r_{\parallel s}(SC_2)$, 27 φ_s(SPtCl), 24 ν_s(PtS)	$r_{\parallel s}(SC_2)$
212 sh		210	202 sh		198	234 sh	234 sh	A″	233	*Pd*: 51 $r_{\parallel a}(SC_2)$, 20 $\varphi(PdS_2)$, 12 $\delta_a(SC_2)$, 11 $\varphi(PdCl_2)$ *Pt*: 77 $r_{\parallel a}(SC_2)$, 14 φ_a(SPtCl), 5 ν_a(PtS)	$r_{\parallel a}(SC_2)$
225 m		226	205 m		209	208 m	208 w	A″	208	88 $r_{\perp a}(SC_2)$, 7 ν_a(MCl)	$r_{\perp a}(SC_2)$
	142 w	138		136 w	132	175 m	173 s	A′	173	*Pd*: 48 $r_{\perp s}(SC_2)$, 45 δ_s(SPdCl) *Pt*: 88 $r_{\perp s}(SC_2)$	$r_{\perp s}(SC_2)$
	186 m	185		181 m	183					53 δ_s(SPdCl), 39 $r_{\perp s}(SC_2)$, 6 $\tau_s(SC_2)$	δ_s(SPdCl)
172 m		173	173 m		176					96 $\varphi(PdCl_2)$ – linear bending	$\varphi(PdCl_2)$
120 s		116	118 s		114					95 $\varphi(PdS_2)$ – linear bending	$\varphi(PdS_2)$
						147 m	147 w	A″	143	72 φ_a(SPtCl) – linear bending, 15 $r_{\parallel a}(SC_2)$	φ_a(SPtCl)
						130 w	134 m	A′	140	53 φ_s(SPtCl) – linear bending, 38 $r_{\parallel s}(SC_2)$	φ_s(SPtCl)
79 s		83	80 s		81					92 δ_a(SPdCl)	δ_a(SPdCl)
						77 s		A′	79	67 $\delta_s(PtL_4)$, 33 $\delta_s'(PtL_4)$	$\delta_s(PtL_4)$[c]
		65			61			A′	52	89 sym MS tors, 9 $\omega_s(SC_2)$	Sym MS torsion
54 m		56	56 m		57					80 δ_a'(SPdCl)	δ_a'(SPdCl)
		44			43	66 sh		A″	62	75 asym MS tors, 9 $\omega_a(SC_2)$	asym MS torsion
						55 m		A″	59	95 $\delta_a(PtL_4)$	$\delta_a(PtL_4)$
								A′	48	58 $\delta_s'(PtL_4)$, 33 $\delta_s(PtL_4)$	$\delta_s'(PtL_4)$

[a] Notations: ν = stretching, δ = bending, τ = twisting, ω = wagging, r = rocking, φ = linear bending, s = symmetric, a = asymmetric modes, ip = in-phase, oop = out-of-phase; ∥ and ⊥ denote direction of dipole moment change *vs.* movement; intensities: vs = very strong, s = strong, m = medium, w = weak, sh = shoulder. [b] PED values refer to non-deuterated complexes. [c] PtL_4 refers to the four equatorial ligand atoms.

Table 3 Experimental vibrational frequencies (cm^{-1}) and refined force constants of the H_3O^+ ion in different systems

		$H_3O^+ \cdots ClO_4^-$ (soln.)[27]		$H_3O^+ \cdots Cl^-$ (soln.)		$H_3O^+ \cdots Me_2SO$ (HCl soln.)	
		Exp.	Calc.	Exp.	Calc.	Exp.	Calc.
A_1	ν_1	3288	3285	3320	3320	3220	3220
E	ν_3	3100	3100	2980	2981	3070	3070
E	ν_4	1577	1577	1705	1705	(1644)	1643
A_1	ν_2	1175	1175	1093	1093	1032	1032
K(OH)[a]		5.797		5.739		5.607	
k(OH, OH)[a]		–0.105		–0.288		–0.063	
H(HOH)[b]		0.594		0.625		0.573	
h(HOH, HOH)[b]		0.049		–0.013		–0.020	

[a] N cm^{-1}. [b] 10^{-18} Nm rad^{-2}.

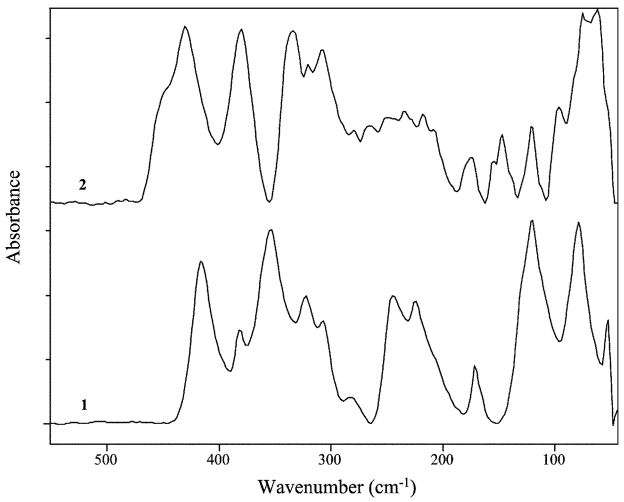

Fig. 4 Far-IR spectra of the solid *trans*-Pd($(CH_3)_2SO)_2Cl_2$ (**1**) and *cis*-Pt($(CH_3)_2SO)_2Cl_2$ (**2**) compounds.

All normal coordinate and force field calculations were performed by means of the PC-based program package developed by Mink and Mink.[14] The results are summarized in Table 3, Table 4 and Table S1.†

X-Ray absorption measurements

Sulfur K-edge X-ray absorption near edge structure (XANES) spectra were recorded at Stanford Synchrotron Radiation Lightsource at beamline 6-2. Details of the measurements are described elsewhere.[15] The energy scale was obtained by setting the lowest energy peak maximum of sodium thiosulfate ($Na_2S_2O_3 \cdot 5H_2O$) to 2469.2 eV, which is the calibration scheme that seems to agree most closely to the calculated values.[16] The liquid samples were held in a 1 mm Teflon spacer between 5 μm sulfur-free polypropylene film windows. The solids were finely ground and dusted on as a thin layer on sulfur-free Mylar adhesive tape.

Computational details

The experimental spectra were evaluated by computing theoretical XANES spectra by means of the Density Functional Theory-Transition Potential (DFT-TP) method, using the same procedure as described elsewhere.[15] No symmetry constraints were imposed on the starting model. The description of the orbital and auxiliary basis sets was for sulfur, carbon, oxygen, hydrogen[16] and chlorine as in our previous studies.[15] For platinum the pseudo potential developed by Küchle *et al.*[17] was used in the representation proposed by Pelissier *et al.*,[18] while for palladium the DZVP (633321/53211/531) orbital description with auxiliary (5,5;5,5) bases was employed. Sulfur atoms other than the core-excited one were described by means of an effective core potential with a [5s,4p,1d] basis set contracted as (311/211/1) to eliminate the S(1s,2s,2p) levels, using a procedure described elsewhere.[15]

Table 4 Variation of S=O stretching frequencies and force constants

	Me_2SO(g)	Me_2SO(l)	Me_2SO(aq)	Me_2SO(HCl)
ν_7/cm^{-1}	1102	1070	1026	987
K(SO)/N cm^{-1}	5.06	4.72	3.98	3.73

Results and discussion

Assignments of vibrational spectra

The SO bond stretching contributes strongly to two fundamental vibrational modes in the dimethyl sulfoxide molecule, at 1102 and 953 cm^{-1} in the gas phase, which usually are assigned as SO stretching and CH_3 rocking after their major components in the potential energy distribution.[1,3,9] In neat liquid dimethyl sulfoxide the former band downshifts to 1070 cm^{-1} due to intermolecular interactions whereas the latter remains nearly unchanged (957 cm^{-1}). Hydration, with formation of a relatively strong $(CH_3)_2SO \cdots HOH$ hydrogen bond, decreases the SO bond strength and leads to downshifts to 1024/1028 cm^{-1} (IR/Raman) and 932/930 cm^{-1} (IR/Raman), respectively. The H_3O^+ interaction with the dimethyl sulfoxide molecule in aqueous HCl solution downshifts the two bands further to 987 and 919 cm^{-1}, respectively (Table 1). The relatively small shifts of the OH stretching frequencies (Table 3) indicate that the type of hydrogen bonding is similar in the three systems studied. The observation of the fundamental frequencies for H_3O^+ in the Me_2SO(HCl) system, especially the umbrella mode at 1032 cm^{-1}, indicates that the H_3O^+ proton is not transferred close to the dimethyl sulfoxide oxygen atom, and the interaction in aqueous HCl solution can be described as $H_3O^+ \cdots OSMe_2$ hydrogen bond. The O–H stretching force constant, 5.607 N cm^{-1}, is smaller than that for 10 mol dm^{-3} HCl, 5.739 N cm^{-1} for $H_3O^+ \cdots Cl^-$, Table 3. The strong hydrogen bonding is also reflected by the very low S=O stretching frequency (987 cm^{-1}) and S–O force constant (3.73 N cm^{-1}) for the Me_2SO(HCl) system, significantly lower than for Me_2SO(aq), Table 4.

The SC_2 asymmetric and symmetric stretching modes are also affected by the interaction of dimethyl sulfoxide with other species. The gas–liquid transition and hydration do not lead to pronounced shifts in the positions of those bands, from 695, 672 cm^{-1} in the gas phase to 700, 670 cm^{-1} for liquid $(CH_3)_2SO$, respectively, but the interaction with a H_3O^+ ion causes a significant increase in the corresponding frequencies, to 727 and 683 cm^{-1}, respectively. Similar tendencies were observed for oxygen-coordinated metal ion complexes,[1–4] and can be explained by an increase in the positive charge on the sulfur atom, while the deformation modes seem less affected.

For the sulfur-coordinated dimethyl sulfoxide solvates the opposite trends would be expected. The assignment of the vibrational bands for *trans*-Pd($Me_2SO)_2Cl_2$ was supported by comparing the experimental spectra of normal and deuterated samples. For *cis*-Pt($Me_2SO)_2Cl_2$ both the band positions and the intensities were compared with those of the palladium complex. In the region around 1100 cm^{-1} where the main SO stretching mode appears, deuteration of *trans*-Pd($Me_2SO)_2Cl_2$ only slightly shifted the medium intensity Raman band to 1110/1117 (H/D) cm^{-1} and the strong IR-band to 1117/1119 cm^{-1}. Deuteration should affect methyl group deformational vibrations, *e.g.*, bendings that usually are observed at higher wavenumbers (1300–1420 cm^{-1}) and rockings at lower (950–1050 cm^{-1}). Hence, the above bands were assigned to the symmetric (Raman) and asymmetric (IR) SO stretching modes of *trans*-Pd($Me_2SO)_2Cl_2$, respectively. For

the platinum complex, the corresponding strong IR and medium intensity Raman bands were found at higher wavenumbers, 1128/1132 cm^{-1}, respectively.

The doublets at 685, 731/688, 729 cm^{-1} (IR/Raman) for the palladium(II) complex shifted significantly upon deuteration to form single bands at lower wavenumbers (644/631 cm^{-1}; IR/Raman) and were attributed to SC_2 stretching vibrations, as also the similar doublets at 696, 737/689, 735 cm^{-1} (IR/Raman) for the platinum(II) complex. The higher frequency bands originate from asymmetric modes and the lower from symmetric modes. The comparison of band intensities in Raman and IR allowed the in-phase (ip) and out-of-phase (oop) modes to be distinguished, see Table 2.

For complexes with sulfur-coordinated dimethyl sulfoxide, characteristic bands at 410–450 and 370–390 cm^{-1} are reported in the literature.[19] We have assigned these features as bending and twisting modes of the coordinated dimethyl sulfoxide molecule, respectively. In the currently studied complexes the corresponding bands were obtained at 416/431 cm^{-1} (IR/Raman) and 449, 430/452, 433 cm^{-1} (IR/Raman) for bending modes and at 382/381 cm^{-1} (IR/Raman) and 376/381, 378 (IR/Raman) cm^{-1} for twisting modes of the palladium and platinum complexes, respectively. Higher frequency bands were assigned as symmetric modes and lower frequency bands as asymmetric. Normal coordinate analysis revealed significant coupling of the bending vibrations with other modes, especially with metal–sulfur stretchings. Deuteration induced well defined low-frequency shifts for these bands as expected from the contribution of the methyl group vibrations in these modes.

The assignment of the bands between 300 and 365 cm^{-1} was less straight-forward because both metal–chloride stretchings and dimethyl sulfoxide wagging modes appear in this region. According to literature data,[20] Pd–Cl stretching vibrations in *trans*-$PdCl_2L_2$ complexes occur at 262–353 cm^{-1}, and Pt–Cl stretchings for *cis*-$PtCl_2L_2$ complexes at 281–374 cm^{-1}, depending on the nature of other ligands (L) and the geometry of the molecule. Our assignment (Table 2) was based on the shifts observed upon deuteration and on the relative intensities of the bands in the Raman and IR spectra.

High polarity of the bond allows significant changes of the molecular dipole moment along the normal mode and promotes high intensity of the corresponding IR absorption band. Therefore, for *trans*-$Pd(Me_2SO)_2Cl_2$ we assigned the strong IR band at 354 cm^{-1} (337 cm^{-1} for the deuterated sample) as the Pd–Cl asymmetric stretching, despite its relatively large shift upon deuteration, see below. The medium intensity IR band at 330 (288) cm^{-1} was attributed to the wagging mode of the ligand. The strongest Raman band at 309 (307) cm^{-1} was assigned as symmetric Pd–Cl stretching and the weak band at 363 (302) cm^{-1} as in-phase wagging. The pronounced shift of the asymmetric Pd–Cl stretching upon deuteration could be explained by its coupling with the dimethyl sulfoxide rocking modes.

The most intense bands in the IR spectra of *cis*-$Pt(Me_2SO)_2Cl_2$ were observed at 335 and 309 cm^{-1}; the high Raman intensity of the former supports the assignment of the high frequency band to the symmetric Pt–Cl stretching mode and the lower frequency band to the asymmetric. This order of the bands ($\nu_s > \nu_a$) is characteristic for the *cis*-MX_2L_2 complexes containing ligands with sulfur donor sites,[20] while for *trans*-complexes the reverse order is more common by far. In this region the dimethyl sulfoxide wagging modes were observed as well, at 320/319 cm^{-1} (IR/Raman). All these skeletal vibrations are shifted to higher wavenumbers in a comparison with neat dimethyl sulfoxide, in contrast to the downshift in oxygen-coordinated complexes.

The metal–sulfur bonding for the palladium(II) and especially the platinum(II) complexes is not very polar, which results in lower intensity of the corresponding IR bands. Also, the coupling of these modes with ligand vibrations (mostly with SC_2 bending and rocking modes) may to some extent decrease their intensity. Based on such considerations, the palladium–sulfur asymmetric stretching mode was assigned as the medium intensity IR band at 246 (245) cm^{-1}, and the symmetric mode as the Raman feature at 160 (152) cm^{-1} that only shifts slightly at deuteration. For the platinum complex the corresponding asymmetric and symmetric modes were observed at 251 cm^{-1} (weak in IR, medium intensity in Raman) and 273 (weak in IR)/275 cm^{-1} (strong in Raman). The lower frequency of the symmetric palladium–sulfur stretching vibration results from the *trans*-influence of the sulfur-coordinated ligands. Similar trends of the frequencies for M–S symmetric and asymmetric stretching modes are observed as for the M–Cl modes: $\nu_s > \nu_a$ for *cis*-complexes, whereas for *trans*-configuration this order is reversed. The larger separation between the symmetric and asymmetric stretching frequencies for the *trans* complex is a result of the stronger vibrational interaction between the ligands in *trans*-positions. The stretch–stretch interaction force constants for both the MCl and MS vibrations are about 3 times larger for *trans*- than for *cis*-complexes (Table S1†). The significantly higher M–S stretching frequency for the platinum complex compared to palladium corresponds to a higher force constant, which reflects the increase in bond covalence. The stronger coordination of sulfur-donor ligands by the platinum atom is consistent with Pearson's hard–soft acid–base principles.[21]

The SC_2 rocking modes were observed as weak to medium spectral features at 225, 212/142, 213 cm^{-1} (IR/Raman) and the linear bendings at 120, 172 cm^{-1} (IR) for *trans*-$Pd(Me_2SO)_2Cl_2$, with corresponding bands at 175, 208, 218, 234/173, 208, 221, 234 cm^{-1} (IR/Raman) and 130, 147 cm^{-1} (IR) for *cis*-$Pt(Me_2SO)_2Cl_2$. Assignments of all observed fundamentals, supported by normal coordinate calculations, together with potential energy distributions, are given in Table 2.

Force field calculations. To follow the trends in the metal–ligand bonding, force constants were calculated (summarized in Table 3, Table 4 and Table S1†) using literature data for the molecular structure,[12,13] and the vibrational spectra of the presently studied compounds. For dimethyl sulfoxide (Me_2SO) the trend in the SO stretching force constant was of particular interest for correlations to the shifts in the SO stretching frequencies: $Me_2SO(g) > Me_2SO(l) > Me_2SO(aq) > Me_2SO(HCl)$. A qualitative explanation of this trend was indicated above. Noteworthy is that the hydrogen bond to the H_3O^+ ion influences the SO bond much more than coordination to metal ions: the SO force constant decreases to 3.73 N cm^{-1} from 4.72 N cm^{-1} in liquid Me_2SO,[3] whereas for some trivalent metal ion solvates the force constants range from 4.17 N cm^{-1} for $Ga(Me_2SO)_6I_3$ to 4.69 N cm^{-1} for $Lu(Me_2SO)_8I_3$.[2–4]

Normal coordinate force field calculations were performed to compare the force constants of square planar MCl_4^{2-} complexes with those of the $M(Me_2SO)_2Cl_2$, M = Pd and Pt, solvates.

Literature data were used for molecular geometry and vibrational spectra.[22–25] The results show higher force constants for the platinum–ligand bonds: for the MCl_4^{2-} species the stretching force constant increases from 1.48 N cm^{-1} (Pd) to 1.80 N cm^{-1} (Pt) without change in the metal–ligand bond distances (2.306 and 2.308 Å for $PdCl_4^{2-}$ and $PtCl_4^{2-}$, respectively).[22,23] For the presently studied $M(Me_2SO)_2Cl_2$ complexes the separation between the Pd–Cl and Pt–Cl force constants is smaller due to the lack of *trans*-influence for M = Pt. The relatively high Pd–Cl force constant for *trans*-$Pd(Me_2SO)_2Cl_2$ is accompanied by a slightly shorter Pd–Cl bond distance than for $PdCl_4^{2-}$ (2.288 *vs.* 2.306 Å), whereas for the platinum(II) complexes the bond distance remains similar (Pt–Cl, 2.309 *vs.* 2.308 Å). The higher force constants of the platinum(II) compounds reflect the higher covalency of the Pt–Cl than the Pd–Cl bonds.

The even higher preference for sulfur-donor ligands in the $M(Me_2SO)_2Cl_2$ complexes for M = Pt(II) than for Pd(II) is reflected in the higher M–S force constant, 2.21 and 1.52 N cm^{-1}, respectively. The much lower Pd–S force constant for *trans*-$Pd(Me_2SO)_2Cl_2$ corresponds to a longer Pd–S bond distance: 2.299 *vs.* 2.236 Å for the platinum(II) complex. The coordination to the sulfur atom of dimethyl sulfoxide increases the S–O stretching force constant, from 4.72 N cm^{-1} for neat Me_2SO to 6.79 and 7.18 N cm^{-1} for the palladium and platinum solvates, respectively. Oxygen coordination leads to lower SO force constants,[2–4] and is a striking difference between O and S coordination. Sulfur coordination also increases the C–S stretching force constants somewhat, from 2.06 N cm^{-1} for neat Me_2SO to 2.22 and 2.27 N cm^{-1} for *trans*-$Pd(Me_2SO)_2Cl_2$ and *cis*-$Pt(Me_2SO)_2Cl_2$, respectively.

Sulfur K-edge X-ray absorption

The experimental sulfur K-edge XANES spectra of the dimethyl sulfoxide solutions in CH_3CN and concentrated HCl are compared with those of the solid samples $M(Me_2SO)_2Cl_2$, M = Pd and Pt, in Fig. 5. The hydrogen bonded H_2O–$H^+ \cdots OSMe_2$ species, which dominates in the highly acidic HCl solution, shows two resolved peaks with similar intensity and a shoulder on the high energy side. The features are centered at about 2472.9, 2474.1 and 2475.3 eV, respectively, while for uncoordinated dimethyl sulfoxide molecules in dilute acetonitrile solution an asymmetric peak is observed at 2473.5 eV with a shoulder at 2475.0 eV. Protonation of the dimethyl sulfoxide molecule could occur either at the sulfur or oxygen atom as for the sulfite (SO_3^{2-}) ion,[15] but since the sulfur atom has a softer character in dimethyl sulfoxide the proton forms a hydrogen bond to the oxygen atom.

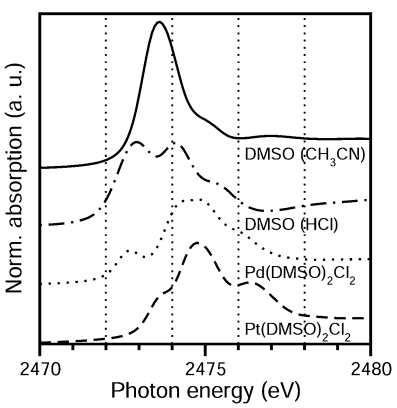

Fig. 5 Normalized sulfur K-edge XANES experimental spectra of 0.05 mol dm^{-3} dimethyl sulfoxide solutions in acetonitrile (—), concentrated hydrochloric acid (-·-), and the solid solvates $Pd((CH_3)_2SO)_2Cl_2$ ($\cdots$) and $Pt((CH_3)_2SO)_2Cl_2$ (---), respectively.

The dimethyl sulfoxide ligands, coordinated *via* the sulfur atom to the divalent metal ions palladium(II) and platinum(II), as in the dichlorobis(dimethyl sulfoxide) solvates, splits the asymmetric peak observed for the free dimethyl sulfoxide molecule. The spectrum of the *trans*-$Pd(Me_2SO)_2Cl_2$ complex with high symmetry shows larger splitting than for *cis*-$Pt(Me_2SO)_2Cl_2$. The X-ray absorption spectrum of the former complex exhibits four peaks resolved at 2472.7, 2474.4, 2474.8 and 2476.0 eV, while the latter solvate displays three features at 2473.8, 2474.8 and 2476.4 eV.

Protonated dimethyl sulfoxide, $(CH_3)_2SOH^+$. For the calculations of theoretical spectra the crystal structure geometry of the protonated dimethyl sulfoxide molecule was used.[26] Different models were constructed by adding one hydrogen bonded water molecule (assuming the H–O bond distance 1.0 Å with tetrahedral HOH angles) in addition to the hydrogen bonding proton placed at 1.12 and 1.3 Å from the dimethyl sulfoxide oxygen atom, *i.e.* forming $H_2OH^+ \cdots OS(CH_3)_2$ or $H_2O \cdots H^+OS(CH_3)_2$ entities, respectively, while keeping the O–H $\cdots$ O distance at 2.414 Å as in the crystal structure (Fig. 6). The theoretical spectra were calculated as described elsewhere,[15,16] applying corrections due to relativistic and relaxation effects as well as an additional empirical shift (–0.5 eV for model A and –0.6 eV for models B and C) of the energy scales to obtain coincidence of the main features in the experimental and theoretical spectra. The overall corrections consisted, for most states, except for the first 9, 6 and 9 states for models A, B and C, respectively (see below), of a shift of these theoretical states to higher energies by 3.23, 3.21, and 3.22 eV for the species: $(CH_3)_2SOH^+$ (model A), $H_2O \cdots {}^+HOS(CH_3)_2$ (model B), and H_2O–$H^+ \cdots OS(CH_3)_2$ (model C), respectively. For each of the first 9, 6 and 9 states corresponding to the models A, B and C, the relaxation energies were calculated and applied individually, while the remaining states were corrected with the mean value for each model of these calculated relaxation energies.

The two experimental spectral features at about 2472.9 and 2474.1 eV are reproduced by transitions **1** and **2** for all three models. The splitting between these states decreases gradually, from 1.6 (A), to 1.2 (B), to 1.1 eV (C), mostly because the 2nd state shifts toward lower energy (Table 5). The experimental shoulder corresponds to transition **3** for models B and C, and to **3** and **4** for model A. In the theoretical spectra for all three models, state **1** is attributed to the transition from S(1 s) to an antibonding σ*(S–O) molecular orbital (MO), and transition **2** to an MO with π*(S–O) bond character. The main discrepancies in the calculated transition energies and intensities are found for the unhydrated model A, where states **3** and **4** are attributed to MOs with σ*(O–H) character and σ*(S–O, S–C) contribution from the two methyl groups. State **3** for model B, mainly with σ*(S–O, S–C) character, resembles state **4** for model A (*cf.* Fig. S1†). The shapes of the MOs for the main transitions for models B and C are also similar to those for the uncoordinated dimethyl sulfoxide molecule.

The character of the MOs of states **1**, **2** and **3** and the corresponding transitions are similar for models B and C. The

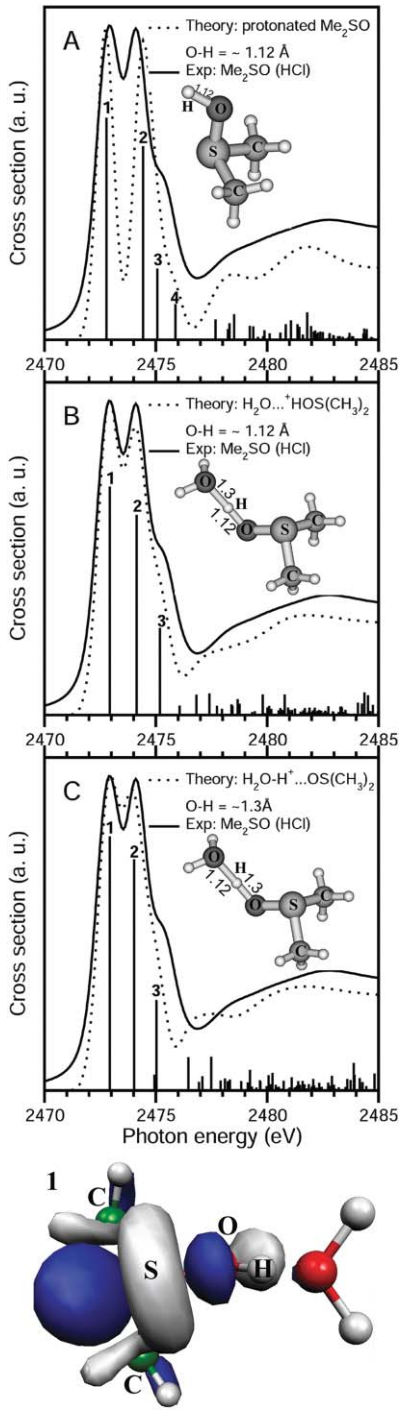

Fig. 6 Theoretical S K-edge XANES spectra (· · ·) calculated for: model **A**, the unsolvated protonated dimethyl sulfoxide molecule; model **B**, solvated with one hydrogen bonded water molecule $H_2O \cdots {}^{+}HOS(CH_3)_2$; and model **C**, $H_2O–H^{+} \cdots OS(CH_3)_2$, and the experimental spectrum of 0.05 M dimethyl sulfoxide in concentrated hydrochloric acid (—). The vertical bars represent the calculated transition energies and cross-sections, convoluted with 0.9 eV (model **A**) and 1.1 eV (models **B** and **C**) FWHM Gaussians below 2476.2 eV, linearly increasing to 8 eV FWHM above 2496.2 eV. The LUMO contour (transition **1**) for models **B** and **C** is shown above, the MOs corresponding to **1**, **2**, **3** and **4** are shown in Fig. S1.†

best match to the experimental spectrum is achieved for model B, even though models A and C also represent the main features satisfactorily. Thus, increasing the distance of the proton from the dimethyl sulfoxide oxygen atom only induces small changes in the energy and intensity of the transitions, and the computed spectrum is not very sensitive to the position of the proton in the hydrogen bond.

***cis*- and *trans*-Isomers of the dichlorobis(dimethyl sulfoxide) platinum(II) complex.** The theoretical XANES spectra were calculated for both isomers of the sulfur-coordinated $Pt((CH_3)_2SO)_2Cl_2$ solvate based on the previously determined geometry.[12,13] The theoretical spectra generated for these species were obtained by applying corrections for relativistic (+7.4 eV) and relaxation effects. The relaxation energy contributions were calculated and applied individually for each of the first nine excited states, while their mean values (–3.32/–3.36 eV for the *cis*- and *trans*-configurations, respectively) were used for the remaining states. A minor additional empirical shift, –0.3 and –0.05 eV, was applied to the convoluted calculated spectra of the *cis*- and *trans*-$PtCl_2(Me_2SO)_2$ complexes, respectively, to match the position of the main peak in the experimental spectra, *cf.* Fig. 7A,B.[16]

The intensity and the corresponding absolute energy values obtained for the first six transitions for both isomers of the $PtCl_2(Me_2SO)_2$ complex are given in Table 6. The resulting theoretical XANES spectra for the geometric isomers of the $PtCl_2(Me_2SO)_2$ complex reproduce reasonably well the experimental features, except for the first low energy peak. The calculated transitions are distributed over a region of 2.3/2.1 eV for the *cis*- and *trans*-species, respectively, and do not properly represent the experimental splitting of about 3.3 eV observed between the near edge features. For both isomers the two most intense peaks, at 2474.8 and 2476.4 eV, were generated by three transitions, **1**, **2**, **3** and **4**, **5**, **6**, respectively. The pseudo potential description of the heavy platinum atom in the calculation seems to be the most likely reason for the relatively poor agreement with the experimental peak for the LUMO transition **1** observed at 2473.8 eV.

The similarity of the calculated spectra for the geometric isomers is also evident when inspecting the shape of the MOs that correspond to the states **1**–**6**. The probability of the LUMO transition **1** is almost unaffected by the change in configuration (Fig. 7A,B and Table 6), but the intensity ratios and energy differences between the remaining transitions are slightly more sensitive. The shape of the LUMO for both isomers is virtually identical, showing delocalization over the platinum and its nearest neighbour atoms and has antibonding σ*(Pt–Cl, Pt–S) character (*cf.* Fig. S2†). The MOs corresponding to transitions **2** and **3** of the *cis*-isomer display mixed antibonding σ*–π* character delocalized over the platinum atom and one of the dimethyl sulfoxide molecules. LUMO + 1 has mainly σ*(S–O) and some π*(Pt–S) character, while LUMO + 2 is dominated by antibonding σ*(S–C) together with some π*(S–O, Pt–S) character. LUMO + 1 and LUMO + 2 for the *trans*-isomer are almost identical displaying mostly σ*(S–C, S–O) with some π*(Pt–S) character. The transition **3**, which has its highest cross-section for the *cis*-isomer, can mainly be attributed to an S(1s) → σ*(S–C) transition, but with the electron charge distributed over several atoms (*cf.* Fig. S2†). The MOs for this isomer corresponding to the states **5** and **6** involve only one of the Me_2SO ligands and are almost identical, exhibiting mainly antibonding σ*(S–C, S–O) character.

Table 5 Energy and intensity of the calculated S(1s) electronic transitions for the following species: $(CH_3)_2SOH^+$ (model A), $H_2O\cdots{}^+HOS(CH_3)_2$ (model B) and H_2O–$H^+\cdots OS(CH_3)_2$ (model C) (Fig. 6A,B,C)

	Energy/eV			Oscillator strength/Mbarn		
Transition no.	Model A	Model B	Model C	Model A	Model B	Model C
1	2472.8	2472.9	2472.9	0.1415	0.1399	0.1292
2	2474.4	2474.1	2474.0	0.1234	0.1226	0.1175
3	2475.1	2475.2	2475.0	0.0454	0.0533	0.0459
4	2475.9	—	—	0.0227	—	—

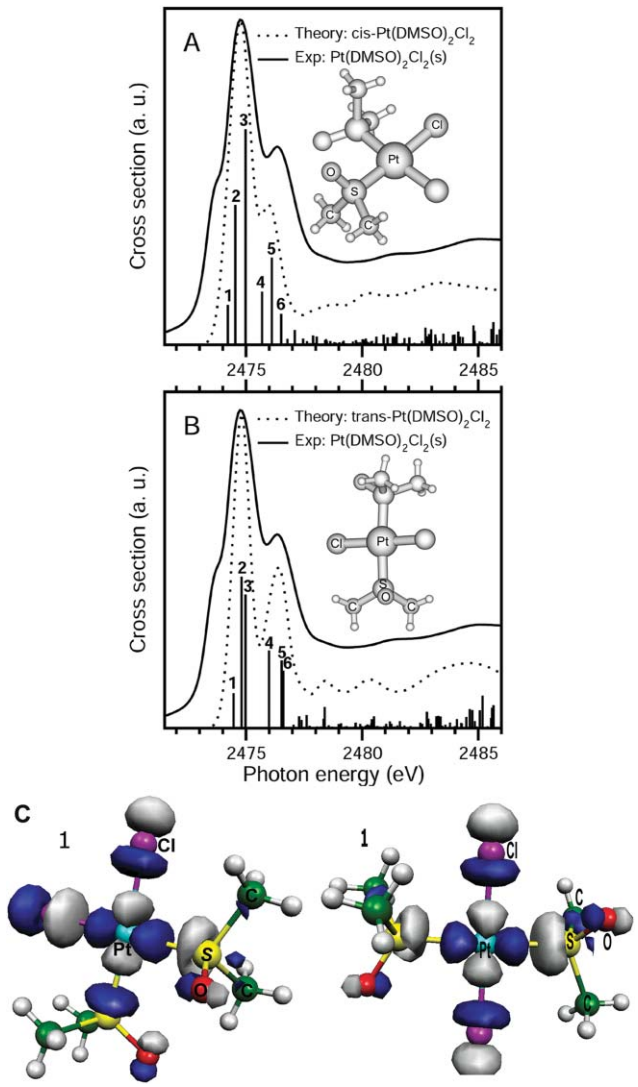

Fig. 7 Calculated S K-edge XANES spectra (···) of the *cis*- (A) and *trans*- (B) isomers of the $Pt((CH_3)_2SO)_2Cl_2$ complex compared with the experimental XANES spectrum of the solid $Pt((CH_3)_2SO)_2Cl_2$ compound (—). The vertical bars represent the calculated transition energies and cross-sections, convoluted with FWHM Gaussians of 0.8/0.8 eV below 2479.1/2479.2 eV, linearly increasing to 8 eV FWHM above 2499.1/2499.2 eV, respectively. The LUMO contours (receiving transition **1**) for the *cis*- and *trans*-isomers are shown in C; all MOs for marked transitions in Fig. S2.†

The MO for the *trans*-isomer corresponding to state **4** has antibonding σ*(S–C, S–O) character, while the distribution of the charge for the orbital associated with transition **6** is very diffuse and has mostly σ*(S–O) and π*(S–O) character. The state **5** is attributed on the other hand to a MO which is mostly dominated by antibonding π*(Pt–S) character.

Table 6 Energy and intensity of the calculated transitions for the *cis*- and *trans*-isomers of the $Pt(Me_2SO)_2Cl_2$ complex (Fig. 7A,B)

	Energy/eV		Oscillator strength/Mbarn	
Transition no.	*cis*	*trans*	*cis*	*trans*
1	2474.2	2474.5	0.0226	0.0209
2	2474.5	2474.8	0.0792	0.0904
3	2475.0	2475.0	0.1221	0.0797
4	2475.7	2476.0	0.0301	0.0463
5	2476.1	2476.5	0.0494	0.0403
6	2476.5	2476.6	0.0175	0.0343

***cis*- and *trans*-Isomers of the dichlorobis(dimethyl sulfoxide) palladium(II) complex.** The molecular geometries used for the calculation of the spectra were derived from the crystal structure of *trans*-isomer.[12] Similar corrections as for the platinum complex were applied for the geometric isomers of the $Pd((CH_3)_2SO)_2Cl_2$ solvate. For both isomers, separate relaxation effects were evaluated and applied to the first nine states and their mean values –2.97/–2.82 eV to the remaining transitions, in addition to the relativistic (+7.4 eV) and additional empirical shifts of –0.5/–0.9 eV for the *cis*- and *trans*-$Pd((CH_3)_2SO)_2Cl_2$ complexes, respectively. The convoluted corrected theoretical spectra obtained for both isomers are displayed in Fig. 8A,B, while the absolute energy and intensity for the transitions marked in these figures are given in Table 7.

The experimental peak observed at 2472.7 eV seems to be best matched by transition **1** computed for the *trans*-isomer (*cf.* Table 7). State **1** is for both isomers attributed to the excitation of the S(1s) electron into the LUMO, which has antibonding σ*(Pd–Cl, Pd–S) character (*cf.* Fig. S3†), involving as for the

Table 7 Energy and intensity of the calculated transitions for the *cis* and *trans* isomers of the $Pd(Me_2SO)_2Cl_2$ complex (Fig. 8A,B)

	Energy/eV		Oscillator strength/Mbarn	
Transition no.	*cis*	*trans*	*cis*	*trans*
1	2473.3	2472.8	0.0188	0.0208
2	2474.2	2473.8	0.0771	0.0790
3	2474.9	2474.8	0.1190	0.1298
4	2475.4	2475.6	0.0412	0.0558
5	2475.9	2475.7	0.0155	0.0251
6	2476.4	—	0.0238	—

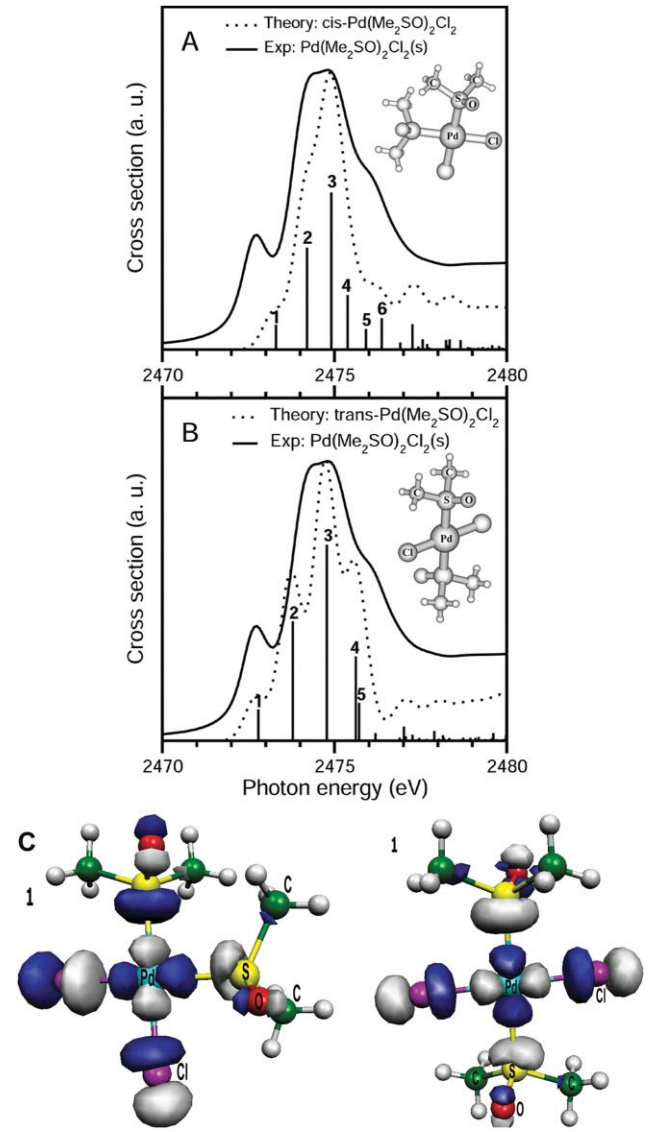

Fig. 8 Calculated S K-edge XANES spectra (···) of the *cis*- (A) and *trans*- (B) isomers of the $Pd((CH_3)_2SO)_2Cl_2$ complex compared with the experimental XANES spectrum of the solid $Pd((CH_3)_2SO)_2Cl_2$ compound (—). The vertical bars represent the calculated transition energies and cross-sections, convoluted with FWHM Gaussians of 0.75/0.75 eV below 2479.2/2478.8 eV, linearly increasing to 8 eV FWHM above 2499.2/2498.8 eV, respectively. The LUMO contours (receiving transition **1**) for the *cis*- and *trans*-isomers are shown in C; all MOs for marked transitions in Fig. S3.†

$Pt((CH_3)_2SO)_2Cl_2$ complex all the sulfur and chlorine atoms. The transitions **2**, **3**, **4** and **2**, **3**, evaluated for the isomeric *cis*- and *trans*-structures, reproduce the experimental peaks appearing at 2474.4 and 2474.8 eV, respectively. The splitting obtained between the states **2** and **3** as well as their absolute energy positions are quite well reproduced for the *cis*-isomer. The states **5** and **6** for the *cis*-isomer and **4** and **5** for the *trans*-isomer correspond to the shoulder observed at 2476.0 eV. For both of the isomers the LUMO + 1 (state **2**) has mainly σ*(S–O) character, but with some minor contribution from antibonding π*(Pt–S) for the *cis*-conformer. The most intense computed transition, **3**, was attributed to S(1 s) → LUMO + 3 for both conformers, but with slightly different mixed antibonding σ*–π* character of the receiving MOs. For the *cis*-isomer the MO is dominated by antibonding σ*(S–C) character with some π*(Pt–S, S–O) contribution involving only one of the Me_2SO ligands, while for the *trans*-isomer the receiving MO is dominated by π*(S–O) as well as some antibonding σ*(S–C) character. LUMO + 4 corresponds for both isomers to transition **4** and has σ*(S–C, S–O) antibonding character. The state **5** transition calculated for the *cis*-isomer occurs into LUMO + 5 that shows mixed contributions of antibonding σ* character between the sulfur, oxygen and one of the carbon atoms belonging the same Me_2SO ligand (*cf.* Fig. S3†). The last transitions marked in Fig. 8A,B, namely **6** and **5** for the *cis*- and *trans*-$Pd((CH_3)_2SO)_2Cl_2$ are attributed to LUMO + 6 and LUMO + 8, respectively. These MOs are quite similar with the charge delocalized over almost the entire molecule with major contributions of σ*(S–O) and some σ*(S–C) antibonding character. Transitions to LUMO + 2 for both isomers, and to LUMO + 5, LUMO + 6 and LUMO + 7 for the *trans*-isomer, have too low intensity to show up in the spectra.

Conclusions

A force field study of the vibrational spectra of strongly hydrogen bonded dimethyl sulfoxide, combined with sulfur K-edge X-ray absorption measurements has been performed to evaluate the effect of the changed charge distribution in the dimethyl sulfoxide molecule. The experimental spectra of dimethyl sulfoxide in concentrated HCl solution are in satisfactory agreement with those calculated for a molecular model of dimethyl sulfoxide with a hydrogen bond to an H_3O^+ ion, Fig. 6c. The effect of the hydrogen bonded proton on the SO bond is much stronger than oxygen-coordination of dimethyl sulfoxide ligands to metal ions. The decrease of the SO force constant is from 4.72 N cm^{-1} in neat liquid dimethyl sulfoxide to 3.73 N cm^{-1} in the protonated species, whereas the values range from 4.17 N cm^{-1} for $Ga(Me_2SO)_6I_3$ to 4.69 N cm^{-1} for $Lu(Me_2SO)_8I_3$.[2–4]

Complete assignments of the fundamental vibrational modes have been achieved for the sulfur-coordinated *trans*-$PdCl_2((CH_3)_2SO)_2Cl_2$, *trans*-$Pd((CD_3)_2SO)_2Cl_2$ and *cis*-$PtCl_2((CH_3)_2SO)_2Cl_2$ complexes. Normal coordinate analyses of the vibrational spectra showed substantial changes from those in neat dimethyl sulfoxide. The sulfur coordination induced upshifts of some intramolecular modes, in contrast to oxygen-coordination for which the SO stretching and all Me_2SO bending modes shift to lower wavenumbers. A significant strengthening of the SO bonds was indicated by the high force constants of the SO stretching mode (6.79 and 7.18 N cm^{-1} for the palladium and platinum complexes, respectively, *vs.* 4.72 N cm^{-1} for neat dimethyl sulfoxide). The higher covalency of the platinum–ligand bonds results in higher frequencies and higher force constants of ML stretching modes, both for M–Cl and M–S bonds, than for the corresponding palladium compounds, even though the bond distances remain similar.

The effects on the electronic state of the dimethyl sulfoxide molecules in these compounds was investigated by means of sulfur K-edge XANES spectroscopy combined with theoretical DFT-TP calculations. The first transition in the spectra occurred at lower energy than for uncoordinated dimethyl sulfoxide but with different character of the receiving LUMOs for oxygen- and sulfur-coordinated species. The high covalency of the Pt–S bonds,

which also is indicated by the highly delocalized receiving LUMOs, resulted in larger energy shifts than for the palladium(II) complex. The differences in the XANES spectra between the geometrical isomers of the dichlorobis(dimethyl sulfoxide) palladium(II) and platinum(II) complexes were found be too small to allow distinction experimentally.

Acknowledgements

We gratefully acknowledge the Swedish Research Council, the Hungarian National Research Foundation (OTKA #K61611) for financial support, the Swedish Institute for the support through the Visby programme, and SSRL for allocation of beamtime. SSRL is operated by the Department of Energy, Office of Basic Energy Sciences. The SSRL Biotechnology program is supported by the National Institute of Health, National Center for Research Resources, Biomedical Technology Program, and by the Department of Energy, Office of Biological and Environmental Research. We thank Professor Lars G. M. Petterson, Stockholm University, for advice in performing the DFT-TP calculations.

References

1 M. Calligaris, *Coord. Chem. Rev.*, 2004, **248**, 351, and refs cited therein.
2 A. Molla-Abbassi, M. Skripkin, M. Kritikos, I. Persson, J. Mink and M. Sandström, *Dalton Trans.*, 2003, 1746.
3 M. Skripkin, P. Lindqvist-Reis, A. Abbasi, J. Mink, I. Persson and M. Sandström, *Dalton Trans.*, 2004, 4038.
4 A. Abbasi, E. Damian Risberg, L. Eriksson, J. Mink, I. Persson, M. Sandstöm, Y. V. Sidorov, M. Yu. Skripkin and A.-S. Ullström, *Inorg. Chem.*, 2007, **46**, 7731.
5 A. R. Davies, F. W. B. Einstein, N. P. Farrell, B. R. James and R. S. McMillan, *Inorg. Chem.*, 1978, **17**, 1965.
6 B. F. G. Johnson, J. Puga and P. R. Raithby, *Acta Crystallogr., Ser. B*, 1981, **37**, 953.
7 E. Alessio, E. Iengo, S. Geremia and M. Calligaris, *Inorg. Chim. Acta*, 2003, **344**, 183.
8 E. Alessio, B. Serli, E. Zangrando, M. Calligaris and N. S. Panina, *Eur. J. Inorg. Chem.*, 2003, **17**, 3160.
9 M. Tranquille and M. T. Forel, *Spectrochim. Acta, Ser. A*, 1972, **28**, 1305.
10 M. Tranquille and M. T. Forel, *Canadian J. Spectrosc.*, 1976, **21**, 11.
11 E. Damian, F. Jalilehvand, A. Abbasi, L. G. M. Pettersson and M. Sandström, *Phys. Scrip.*, 2005, **T115**, 1077.
12 M. J. Bennett, F. A. Cotton, D. L. Weaver, R. J. Williams and W. H. Watson, *Acta Crystallogr.*, 1967, **23**, 788.
13 R. P. Shibaeva, *Koord. Khim.*, 1985, **11**, 129.
14 J. Mink and L. M. Mink, *Computer Program System for Vibrational Analyses of Polyatomic Molecules* (in Lahey-Fujitsu Fortran Win32), Stockholm, 2004.
15 E. Damian Risberg, L. Eriksson, J. Mink, L. G. M. Pettersson, M. Yu. Skripkin and M. Sandström, *Inorg. Chem.*, 2007, **46**, 8332.
16 E. Damian Risberg, F. Jalilehvand, B. O. Leung, L. G. M. Pettersson and M. Sandström, *Dalton Trans.*, submitted.
17 W. Küchle, M. Dolg, H. Stoll and H. Preuss, *Mol. Phys.*, 1991, **74**, 1245.
18 M. Pelissier, N. Komiha and J. P. Daudey, *J. Comput. Chem.*, 1988, **9**, 298.
19 L. V. Konovalov and Yu. N. Kukushkin, *Russ. J. Coord. Chem.*, 1997, **23**, 885.
20 J. Mink and P. L. Goggin, *Kemiai Közlemények.*, 1984, **61**, 275.
21 R. G. Pearson, *Chemical Hardness – Applications from Molecules to Solids*, Wiley-VCH, Weinheim, 1997.
22 H. Takazawa, S. Ohba and Y. Saito, *Acta Crystallogr., Ser. B*, 1988, **44**, 580.
23 S. Ohba, S. Sato and Y. Saito, *Acta Crystallogr., Ser. B*, 1983, **39**, 49.
24 L. A. Degen and A. J. Rowlands, *Spectrochim. Acta, Ser. A*, 1991, **47**, 1263.
25 P. L. Goggin and J. Mink, *J. Chem. Soc., Dalton Trans.*, 1975, 381.
26 J. S. Jaswal, S. J. Rettig and B. R. James, *Can. J. Chem.*, 1990, **68**, 1808.
27 R. C. Taylor and G. L. Vidale, *J. Am. Chem. Soc.*, 1956, **78**, 5999.

